THE JOURNAL OF PHYSICAL CHEMISTRY B

ARTICLE

pubs.acs.org/JPCB

DFT/MM Description of Flavin IR Spectra in BLUF Domains

Benjamin Rieff, Sebastian Bauer, Gerald Mathias, and Paul Tavan*

Lehrstuhl für Biomolekulare Optik, Ludwig-Maximilians-Universität, Oettingenstr. 67, 80538 München, Germany

Supporting Information

ABSTRACT: A class of photoreceptors occurring in various organisms consists of domains that are blue light sensing using flavin (BLUF). The vibrational spectra of the flavin chromophore are spectroscopically well characterized for the dark-adapted resting states and for the light-adapted signaling states of BLUF domains in solution. Here we present a theoretical analysis of such spectra by applying density functional theory (DFT) to the flavin embedded in molecular mechanics (MM) models of its protein and solvent environment. By DFT/MM we calculate flavin spectra for seven different X-ray and NMR structures of BLUF domains occurring in the transcriptional antirepressor AppA and in the blue light receptor B (BlrB) of the purple bacterium *Rb. Sphaeroides* as well as in the phototaxis photoreceptor Slr1694 of the cyanobacterium *Synechocystis*. By considering the dynamical stabilities of associated all-atom simulation models and by comparing calculated with observed vibrational spectra, we show that two of the considered structures (both AppA) are obviously erroneous and that specific features of two further crystal structures (BlrB and Slr1694) cannot represent the states of the respective BLUF domains in solution. Thereby, the conformational transitions elicited by solvation are identified. In this context we demonstrate how hydrogen bonds of varying strengths can tune in BLUF domains the C═O stretching frequencies of the flavin chromophore. Furthermore we show that the DFT/MM spectra of the flavin calculated for two different AppA BLUF conformations, which are called Trp_{in} and Met_{in}, fit very well to the spectroscopic data observed for the dark and light states, respectively, if (i) polarized MM force fields, which are calculated by an iterative DFT/MM procedure, are employed for the flavin binding pockets and (ii) the calculated frequencies are properly scaled. Although the associated analysis indicates that the Trp_{in} conformation belongs to the dark state, no clear light vs dark distinction emerges for the Met_{in} conformation. In this connection, a number of methodological issues relevant for such complex computations are thoroughly discussed showing, in particular, why our current descriptions could not decide the light vs dark question for Met_{in}.

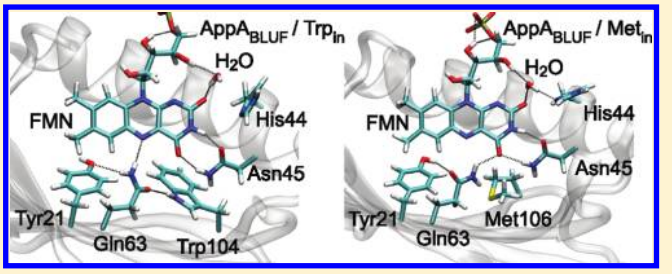

INTRODUCTION

Biological photoreceptors mediate the responses of living organisms to environmental light conditions. Whereas photoreceptors such as the rhodopsins, phytochromes, and xanthopsins employ cofactors featuring light-induced isomerizations,[1] a class of blue-light receptors, which covers the photolyases,[2] the cryptochromes,[3] the so-called LOV[4] (light-oxygen-voltage sensing), and BLUF[5] (blue light sensing using flavin) domains, utilizes the stiff flavin dyes. These flavin chromophores, whose chemical core motif[6] is depicted in Figure 1c, generate the respective biological function through light-induced redox reactions.[1] The reactions can be monitored in a temporally resolved fashion by vibrational spectroscopy.[7] The corresponding spectra can provide information on the flavin redox states[8] and on the conformational changes in the flavin binding pockets, if they can be decoded by a sufficiently accurate computational method. Such a method must be capable of relating the chromoprotein structures, which have to be known at atomic resolution from X-ray crystallography or multidimensional nuclear magnetic resonance (NMR) measurements, to the chromophore spectra determined by infrared (IR) or resonance Raman (RR) spectroscopy.

Computational hybrid methods,[9,10] which combine a density functional theory (DFT)[11,12] description of the respective chromophore with a molecular mechanics (MM) model of its protein environment, are accurate enough to master the task specified above,[13,14] if the applied MM force field is of sufficient quality. Unfortunately, however, the latter condition is not necessarily guaranteed, as long as standard nonpolarizable MM force fields such as CHARMM22,[15] AMBER,[16] or GROMOS[17] are used to describe the condensed phase environment of the chromophore.

In the case of bacteriorhodopsin (BR), for instance, the quite rigid hydrogen bonded network within the binding pocket of the retinal chromophore turned out to be unstable in molecular dynamics (MD) simulations with the quoted standard force fields (see the discussion on pp 10484−6 in ref 18). Correspondingly, DFT/MM calculations of the chromophore IR spectra yielded quite inaccurate descriptions with CHARMM22.[19] However, BR became structurally stable in MD simulations, which employed a new BR specific polarized force field that had been

Received: May 10, 2011
Revised: July 15, 2011
Published: September 02, 2011

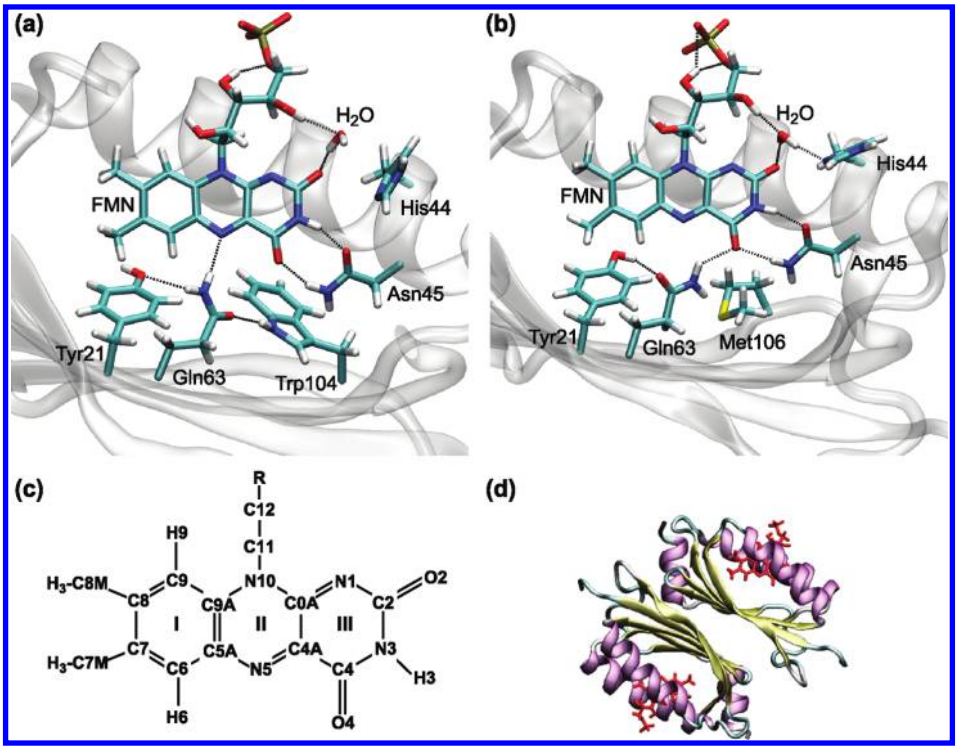

Figure 1. All-atom structures of the active sites in AppA BLUF domains derived by strongly restrained MD simulations (see the Methods section) from (a) the so-called Trp_{in}[21] and (b) the Met_{in}[39] X-ray structural models. The black dotted lines indicate hydrogen bonds between the flavin chromophore and residues of the apoprotein. Panel c depicts the chemical structure and the atom labels of oxidized isoalloxazine, which is the core motif of all flavins,[6] and panel d illustrates the dimeric structure of the AppA BLUF domain.[21,39] The illustrations in a, b, and d were generated with VMD.[40]

generated by iteratively computing[20] new partial charges for the binding pocket with a DFT/MM technique.[18] Furthermore, also the IR spectrum calculated by DFT/MM for the chromophore closely reproduced the observations as soon as the polarized force field was used to model the charge distribution in the chromophore binding pocket.[19]

Taking the BLUF domains as a further example, it is the purpose of this contribution to check whether the quoted failure of standard force fields concerning the DFT/MM description of a chromophore vibrational spectrum was just bad luck (and, thus, restricted to BR) or whether similar failures should be generally expected. Concurrently, we want to pave the way toward high-quality descriptions of the IR spectra of BLUF chromophores. In combination with observed IR spectra such descriptions should be capable to provide (i) answers to the question to what extent given crystal structures represent the solution structures of the IR measurements and (ii) possibly even insights into the details of the conformational changes leading from the initial dark-adapted states to the final light-adapted signaling states of BLUF domains.

Partially supported by X-ray structural models, NMR data, vibrational or UV/vis spectra, and/or quantumchemical calculations various detailed models have been suggested for the dark-light transition in BLUF domains.[21−33] As a common feature these models describe reorganizations of the hydrogen bonded networks, which are supposedly caused by light-induced redox reactions within the flavin binding pockets. The reactions involve the electronically excited flavin as the primary electron acceptor.[22,30] A subsequent proton transfer results in the transient formation of a neutral flavin radical. These charge transfer processes cause a rearrangement of the initial hydrogen bonded network. In particular, the final signaling state features a new or strengthened hydrogen bond to the flavin O4 atom[34−36] as is witnessed by a 17 cm^{-1} redshift of the flavin C4═O4 stretching band.[34−38]

For the AppA (activation of photopigment and Puc expression A) protein from the purple bacterium *Rb. Sphaeroides*, which contains the most intensely studied BLUF domain, two significantly different molecular models were determined by X-ray crystallography and are deposited in the Protein Data Bank (PDB, http://www.rcsb.org). One pertains to the wild-type[21] (PDB-code: 1YRX) and is shown in Figure 1a[40] and the other to the C20S mutant[39] [PDB-code: 2IYG, Figure 1b[40]]. In the wild-type AppA BLUF model,[21] the conserved residue Trp104 is buried in the flavin binding pocket. Therefore, the corresponding BLUF conformation is called "Trp_{in}" [Figure 1a]. In contrast, in the C20S mutant, Trp104 is found at the protein surface,[39] and Met106 takes its position close to the flavin ["Met_{in}", Figure 1b]. Additionally, the orientation and hydrogen bonding pattern of Gln63 is different in the two conformations. Assuming that one of the conformations represents the dark state (e.g., Trp_{in}) and, possibly, the other the light state various intermediate states and mechanistic transformation models have been postulated for the dark-light adaptation process.[21−33] Up to now there is no experimental evidence that clearly favors one of these suggestions.

On the other hand, for various BLUF domains the vibrational spectra of the dark and light states have been characterized in several steady state studies.[34−38] Furthermore, also the kinetics of the dark-light conversion has been carefully investigated by time-resolved UV/vis-pump/IR-probe spectroscopy.[22,30] If one should be able to decode these spectra in terms of structure by reliable DFT/MM calculations one might even be able to assign

larger or smaller degrees of plausibility to the various experimental BLUF structures and theoretical mechanistic suggestions and this is, as mentioned further above, the BLUF specific aim of our endeavor.

In two preceding DFT/MM studies on the flavin IR spectra,[8,41] we have recently presented some of the basic preparatory work, which is required to reach this aim. These studies addressed the IR spectra of oxidized[41] and reduced[8] flavins in aqueous solution, for which a substantial experimental data basis is available in the literature.[42−51] Here, we have predicted the solvatochromic shifts, which should be found in the flavin vibrational spectra upon transfer from the gas phase into a highly polar and isotropic condensed phase environment. For oxidized flavin in water, we have derived a frequency scaling factor applicable to the specific DFT/MM approach used by us which brings the calculated IR frequencies close to the experimental ones.[41]

As expected, this scaling factor turned out to be transferable from the oxidized to the reduced flavins in water, because neither the DFT approach nor the MM force field were changed in this transition. When extending the DFT/MM description to the IR spectra of flavins embedded in protein binding pockets, however, the transferability of the frequency scaling becomes uncertain, because the MM force field for a protein is not necessarily compatible with a given MM model for water. Thus, it remains to be seen to what extent the frequency scaling factor derived from flavins in MM water actually can be extended to flavins in MM models of proteins. Further below we will initially assume transferability, which will be critically addressed later.

The vibrational spectra of flavins solvated in water[45−49] are strikingly similar to those of flavins in dark-adapted BLUF domains.[34−38] For our computational DFT/MM study this finding implies that an oxidized flavin in water, whose DFT/MM spectra and charge distribution were previously calculated by us,[41] should represent a reasonable model for an oxidized flavin mononucleotide (FMN) in dark-adapted BLUF domains.

In the following DFT/MM study on the IR spectra of oxidized flavin in BLUF domains, we will not only consider the two X-ray structures of AppA BLUF quoted above but also two further structural models for this protein[25,39] (PDB-codes: 2IYI and 2BUN) as well as X-ray structures of the BLUF proteins BlrB[52] (Blue light receptor B, PDB-code: 2BYC) from *Rb. Sphaeroides* and Slr1694[24] (PDB-code: 2HFO) from the cyanobacterium *Synechocystis* sp. PCC6803. Before presenting and discussing our computational results, we will first sketch the applied methods.

METHODS

Like in our preparatory work,[8,41] we used for the MM-MD simulations the program package EGO,[53] which treats the electrostatics by the fast structure-adapted multipole method[54,55] combined with a reaction field correction[53] thus implementing toroidal boundary conditions.[56] Furthermore, EGO can speed up the integration by a multiple time step algorithm[57,58] and, here, we applied a basic time step of 1 fs. Berendsen thermo- and barostats[59] were employed to control the temperature T and pressure p, respectively. For MD simulations in the *NVT* ensemble we chose T = 300 K with a coupling time of 0.5 ps, in the *NpT* ensemble we additionally steered p to the target value of 1 bar with a coupling time of 5 ps and an isothermal compressibility of 0.46 GPa^{-1}.

As previously,[8,41] the DFT/MM calculations were carried out with the hybrid method originally suggested in ref 9, which provides an interface between the MM-MD program EGO[53] and the plane-wave DFT code CPMD.[60] Following earlier work[8,13,19,41] we denote the DFT/MM approach applied to FMN in BLUF domains by "MT/BP", because it combines the norm-conserving pseudopotentials of Martin and Troullier[61] with the gradient-corrected exchange functional of Becke[62] and the correlation functional of Perdew.[63] For the MT/BP approach a plane-wave cutoff of 70 Ry has been established as a reasonable choice for computations of flavin vibrational spectra.[41]

Whereas our preparatory DFT/MM calculations on flavins in water were restricted to lumiflavin[8,41] (LF), the BLUF domains contain the somewhat larger FMN molecules as chromophores. To keep the size of the DFT fragment in the DFT/MM treatments of BLUF domains at the reduced size of the LF molecule, we have cut the covalent bond between the atoms C11 and C12 within FMN's ribityl-5′-phosphate side chain [see Figure 1c] using the so-called "scaled position link atom method"[9] (SPLAM). Thus, the DFT fragment was effectively a LF molecule connected through SPLAM to the remainder of the ribityl-5′-phosphate side chain. Note here that a MM force field for the FMN chromophore is given in ref 41. The rectangular box containing the grid for the plane-wave expansion of the Kohn−Sham orbitals was placed around the DFT fragment in such a way that no DFT atom came closer than 3 Å to one of the faces and that the box volume became minimal.

The IR spectra of FMN in BLUF domains were calculated using the protocol[13] for "instantaneous normal mode analysis" (INMA), which has been established as a viable tool for the DFT/MM computation of condensed phase IR spectra in several applications.[8,14,19,41,64−66] Here, a normal-mode analysis is applied to the DFT fragment (LF) embedded in a MM environment (solvated BLUF protein), which is kept fixed at a given structural snapshot. Thus, the FMN can move during the DFT/MM energy minimization in the rigid binding pocket of a BLUF protein and the DFT/MM normal-mode analysis is executed at the optimized geometry. Because a minimum of the potential energy surface is reached in the configurational subspace spanned by the coordinates of the atoms in the DFT fragment, all frequencies are positive like in the usual normal-mode analysis of isolated molecules. For each IR spectrum the normal modes were identified by an automated mode classification procedure.[41]

As is common in theoretical vibrational spectroscopy,[67−69] the calculated DFT/MM frequencies were scaled. Initially we used the scaling factor 1.031. This factor had been derived[41] by comparing vibrational frequencies measured for flavins in aqueous solution with the MT/BP description of LF in a MM water environment, which had been modeled by Jorgensen's "transferable interaction potential using three points" (TIP3P).[70]

Setup of Simulation Models for BLUF Domains. To generate MD simulation models of BLUF domains solvated in TIP3P water, we extracted from the PDB the experimental BLUF structures listed in Table 1. The table characterizes the structures by their PDB codes and by the names of the various proteins enumerated at the end of the Introduction. It distinguishes Trp_{in} from Met_{in} conformations (conf.). Figure 1, panels a and b, provides examples for these conformations. Furthermore, the table gives the assignment of the respective authors, whether their structure is supposed to represent the dark-adapted resting state or the light-adapted signaling state. Finally, the table introduces new names for the various structures, which encode the associated protein name (A/B/S for AppA/BlrB/Slr1694), the conformation (T/M for Trp_{in}/Met_{in}), and the state

Table 1. Experimental BLUF Structures.[a]

PDB code	protein	conf.	state	name
1YRX[21]	AppA	Trp_{in}	dark	ATD
2BUN[25]	AppA	Trp_{in}	dark	ATD*
2IYG[39]	AppA	Met_{in}	dark	AMD
2IYI[39]	AppA	Met_{in}	light	AML
2BYC[52]	BlrB	Met_{in}	dark	BMD
2HFO[24]	Slr1694	Met_{in}	light	SML

[a] 2BUN is from NMR, the others from X-ray; all crystal structures are chain A of the respective sets.

(D/L for dark/light). Note that the new name chosen for the single NMR structure 2BUN[25] is highlighted by an attached star, i.e., this structure is denoted as ATD*.

All PDB entries contain multiple copies of BLUF structures, because the proteins crystallized as multimers. We generally chose chain A. Specifically in the case of entry 2IYI this choice was motivated by a discussion in the original publication of Jung et al.,[39] which claimed that in this case chain A, which structurally differs from chain B, is a more likely model for the light-adapted state. In the case of the NMR data, we have arbitrarily chosen the first structure from the set of 20 geometries deposited under the name 2BUN in the PDB. We consider this structure as a typical representative for the NMR results.

The atom positions for all hydrogens and for other atoms, which are missing in the chosen PDB data sets, were added with the help of the MD program X-PLOR.[71] Here the acidic (Asp, Glu) and basic (Arg, Lys) residues in the various BLUF structures were chosen to be ionized, because they are located close to the water exposed protein surfaces.

In the AppA structures solely the protonation state of His44, which is close to the C2═O2 group of FMN, seemed to be questionable. While the NMR solution structure 2BUN contains a protonated His44, the authors of this structure claim in the associated description[25] that "no positively charged side chains are near C2═O2 in the solution structure of AppA" (p 192), which is an obvious contradiction. Furthermore, in the BlrB structure[52] His44 is replaced by Arg32, which should be positively charged, whereas the Slr1694 structure[24] solely features the polar Asn34 at this position. Due to this uncertainty we generated for AppA structures two alternative all-atom simulation models, one with a positively charged and one with a neutral His44. The models with a protonated His44 are distinguished by appending a "P" to the respective name (cf. Table 1 for the names, to which a "P" is appended).

Next, we embedded the all-atom MD simulation models of the BLUF proteins into periodic water boxes pre-equilibrated in the *NpT* ensemble (T = 300 K, p = 1 bar, see further above) by removing overlapping water molecules. The boxes were shaped as orthorhombic dodecahedra with inner radii of about 40 Å and contained 12 428 rigid TIP3P water molecules before the embedding. Note here that (for both His44 protonation states) the AppA structures ATD, AMD, and AML were modeled as dimers to preserve the hydrophobic interfaces between the β-sheets of the monomeric BLUF units [see Figure 1d]. Only the NMR structure ATD* was modeled as a monomer, because a dimeric structure is not available in this case.

To check whether the choice of monomeric and dimeric simulation models affects the predictions of the FMN vibrational spectra we additionally embedded an AMD monomer into the TIP3P box. Also BMD and SML were constructed as monomers, because here the hydrophobic β-sheet surfaces of the BLUF domains are separated by two additional α-helices from the solvent.[24,52]

If not explicitly stated otherwise we applied the CHARMM22 force field[15] to the BLUF MD simulation systems. In the MM fragments the bond lengths of all hydrogen atoms were kept fixed by the M-SHAKE[72] algorithm.

Restrained Equilibrations of the MD Simulation Models. To preserve the experimental BLUF structures as much as possible during the generation of equilibrated MD simulation models we adopted the following procedure. First the hydrogen and the other modeled protein atoms were adjusted to the experimental structures by short energy minimizations during which the positions of the crystallographic atoms were kept fixed. Coupling the thermostat *exclusively* to the solvent,[73] like in all subsequent MD simulations, and keeping the BLUF domains rigid the solvent was allowed to adjust to the protein volume during 100 ps MD simulations in the *NVT* ensemble. The pressure of the solvent surrounding the rigid BLUF models was subsequently relaxed toward its 1 bar target value in 300 ps *NpT* simulations.

Then all heavy BLUF atoms were softly restrained to the experimental coordinates $\mathbf{r}_c$ by harmonic potentials $k_c(\mathbf{r} - \mathbf{r}_c)^2$. Depending on the location of the respective heavy atom within the protein structure we used two different harmonic force constants. For atoms in the backbone the force constant k_c was set to 6 kcal/(mol Å^2) representing a quite stiff restraint. A value of 2 kcal/(mol Å^2) was chosen for the atoms in the side chains and in FMN, which is a much softer restraint. At the target temperature T = 300 K these potentials restrict the atomic thermal fluctuations to root-mean-square-deviations (RMSDs) of about 0.32 and 0.55 Å, respectively. The softly restrained and solvated protein structures were then simulated for 600 ps in the *NpT* ensemble. Here, measuring the uncontrolled temperature of the BLUF domains served as a check, whether the heat bath (represented by the solvent) properly thermalized the solute protein.[73] Finally the barostats were switched off and further 200 ps were simulated in the *NVT* ensemble for data acquisition (storage every 10 ps). From the resulting 20 snapshots we selected for each BLUF model the snapshot featuring the best match with the respective experimental BLUF structure.

Figure 1, panels a and b, shows for ATD and AMD, respectively, the best matching structures resulting from these restrained MD (rMD) equilibrations. Note that the hydrogen bonds indicated in this figure were defined by the following conditions: the donor−acceptor (D-A) distance is shorter than 3.3 Å and the D-H-A angle is 130° or larger.

Polarized Force Fields for the BLUF Models. As explained in the Introduction the X-ray structure of BR was recently shown to be unstable in extended MD simulations, which applied standard (nonpolarizable) MM force fields.[18] Interestingly such a structural decay was observed once again by us in extended and unrestrained CHARMM22-MD simulations of an AMD dimer in TIP3P water. To speed up the sampling, we had applied for 10 ns a replica-exchange solute tempering approach,[74,75] which showed a large scale motion of Tyr21 within the binding pocket away from its original position [cf. Figure 1b] toward a seemingly much more stable alternative position (data not shown). Note that a similar decay of the hydrogen bonded network stabilizing the flavin binding pocket of BLUF domains was found in

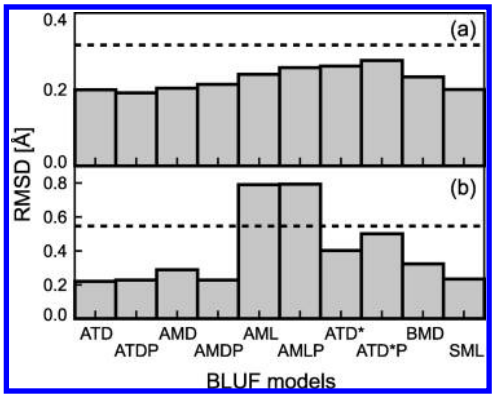

Figure 2. RMSDs between experimental and best matching rMD equilibrated structures for (a) the backbone and (b) side chains in the protein binding pocket for the BLUF models studied here (nomenclature see Table 1). The black dotted lines show the deviations expected at T = 300 K for thermal motion within the soft potentials restraining the positions of the respective heavy atoms.

previous 500 ps CHARMM27-MD simulations of a BlrB model.[32] Here the authors tried to fix the problem by simply adding a water molecule.

Assuming instead that the lacking stability of a hydrogen bonded network in BLUF domains has the same cause as in BR,[18] where it was identfied as the lacking electronic polarizability of standard protein force fields, we decided to copy the same healing strategy that was proven to be successful for BR.[18] Correspondingly we generated polarized force fields (PFFs) for the considered BLUF models by iteratively recalculating "electrostatic potential" (ESP)[76] partial charges of the amino acid side chains surrounding the isoalloxazine in the best matching rMD equilibrated model structures through the DFT/MM approach characterized further above. When the residues Tyr21, Ser41, His44, Asn45, Phe61, Gln63, Asp82, Arg84, His85, and Trp104/Met106 as defined by the AppA numbering for polarization were chosen, the respective DFT fragments consisted of the side chains whose covalent linkages to the backbone were cut at the $C_\alpha - C_\beta$ bonds using SPLAM. We additionally included the special water molecule, which in the AppA BLUF models is hydrogen bonded to FMN-O2 [cf. panels a and b in Figure 1], into the set of polarized molecular groups. The iterative DFT/MM calculation of the ESP partial charges was finished after an approximate self-consistency, as specified by the convergence criterion of ESP partial charge changes smaller than 0.01 e, had been reached for the chosen set. In this paper, the PFFs are mainly utilized in our DFT/MM calculations on the vibrational spectra of BLUF chromophores, where the respective polarized BLUF models are labeled by the subscript "p", i.e., as ATD_p, AMD_p, and so on. We note, however, that unrestrained PFF-MD simulations of the AMD_p dimer showed an enhanced structural stability of the FMN binding pocket (data not shown).

RESULTS AND DISCUSSION

Before calculating the IR spectra of FMN in the various BLUF models by DFT/MM, we checked to what extent the best matching simulation models, which were generated by the careful rMD equilibrations described above, retained the geometries of the experimental parent structures. As measures we calculated RMSDs for the experimentally defined positions of protein atoms. Whenever the electrostatic and van der Waals interactions added by the CHARMM22 force field are incompatible with the experimentally suggested BLUF geometry, the deviations of the rMD equilibrated model from its parent structure will be larger than the expectation values associated with the softly restraining potential at the given temperature T = 300 K (values given above) .

Stability Analysis of the rMD Equilibrated BLUF Structures. We measured the compatibility of the experimental BLUF structures with the all-atom simulation models as described by the CHARMM22 force field using two different RMSDs, one for the heavy atoms in the backbone and the other for the heavy atoms in the side chains of the important residues Tyr21, His44, Asn45, Gln63, and Trp104/Met106 (AppA numbering) determining the structure of the FMN binding pocket [see Figure 1, panels a and b].

Figure 2a shows the RMSDs for the backbones and Figure 2b for the side chains enumerated above. The black dotted lines are the deviations expected for free thermal fluctuations within the respective restraining potentials. According to Figure 2a the backbone geometries of all experimental BLUF models comply with CHARMM22 as is witnessed by the fact that all backbone RMSDs are smaller than the thermally expected deviation. For the side chains Figure 2b demonstrates that most of the best matching rMD equilibrated models remain quite close to their experimental parents. Notable exceptions are the AML and AMLP models,[39] which exhibit RMSDs larger than the thermal limit indicating that they are destabilized by strong forces. Judging from these RMSDs one might additionally argue that the NMR structures[25] ATD*(P) are only marginally stable.

The physical nature of the forces destabilizing the rMD equilibrated models AML and AMLP is analyzed in the Supporting Information (SI). Here we provide in Figure S11 for ATD(P), AMD(P), and AML(P) visual comparisons between the experimental and the rMD equilibrated structures. An accompanying text discusses the structural changes, which are visible in these figures and are caused by the rMD equilibrations. The discussion concludes that the X-ray model AML,[39] as opposed to the other two X-ray structures ATD and AMD, is incompatible with the electrostatics. Therefore we excluded the implausible X-ray structure AML from further consideration.

At this point one may ask whether the structurally different chain B of the PDB entry 2IYI[39] would have been a better choice than the dynamically instable chain A ("AML"). Denoting the all-atom simulation model of chain B as AML_B we found that this model is dynamically as stable as AMD (data not shown). On the other hand, it is also structurally extremely similar to AMD, particularly with respect to the hydrogen bonded network stabilizing the FMN in the AppA-BLUF binding pocket [cf. Figure 1b]. Therefore one is led to assume that IR spectra calculated by the DFT/MM technique for AMD and AML_B will be extremely similar. We checked this issue and found that the C═O stretching frequencies of FMN in AMD and AML_B differed by at most 1 cm^{-1}(data not shown). Therefore, we took AMD as the representative for the type of hydrogen bonded network found at the FMN in the AMD and AML_B models of AppA-BLUF.

Note here that panels a and b of Figure 1 depict the best matching rMD equilibrated models ATD and AMD, respectively. In both cases the rMD representatives are nearly identical to the respective parent X-ray structures (see the discussion of Figure S11 in the SI for further details).

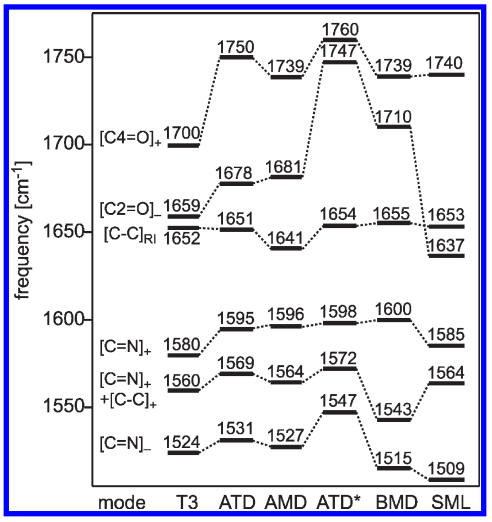

Figure 3. DFT/MM vibrational frequencies of FMN in the rMD equilibrated BLUF proteins ATD, AMD, ATD*, BMD, and SML as described by the CHARMM22 force field.[15] In the AppA models His44 is chosen as unprotonated. As a reference the DFT/MM frequencies of LF in TIP3P water[41] are shown in column T3. All frequencies are scaled by 1.031.[41]

Vibrational Frequencies of FMN in rMD Equilibrated BLUF Models. As mentioned in the Introduction, the spectral positions of the flavin vibrational bands hardly change upon transfer from aqueous solution[45−49] into dark-adapted BLUF domains.[34−38] Computing from the quoted publications average frequencies for all those vibrational flavin bands, which are observed in the 1500−1750 cm^{-1} spectral range, we determined that the two sets of experimental average frequencies (water vs dark-adapted BLUF) deviate by a rmsd of only 1.4 cm^{-1}. Therefore one is lead to expect that such a similarity should show up also in the IR spectra, which are computed by DFT/MM for flavins in TIP3P water and in CHARMM22 models of BLUF domains, respectively. Based on this expectation we initially took our previous DFT/MM results on the IR spectra of fully oxidized LF[41] in TIP3P water as a reference for our new computational results on the IR spectra of FMN in the rMD equilibrated BLUF models.

Figure 3 displays DFT/MM derived and scaled normal-mode frequencies of FMN in the rMD equilibrated BLUF models of AppA (ATD,[21] AMD,[39] ATD*,[25] and unprotonated His44), BlrB (BMD[52]), and Slr1694 (SML[24]). Column T3 depicts the scaled reference spectrum of LF in TIP3P water.[41] The subscripts "+" and "−" at the mode labels [X−Y] denote in-phase and out-of-phase relations, respectively, among the stretches of bonds X−Y contributing to the normal modes. The subscript "RI" points to ring I of isoalloxazine [cf. Figure 1c].

As a most conspicuous feature, all BLUF models show a flavin $[C4{=}O]_+$ frequency, which is strongly blueshifted with respect to the T3 reference. Somewhat smaller blueshifts are predicted for all $[C{=}N]_+$ frequencies. In contrast the shifts of the $[C2{=}O]_-$ frequency exhibit strong differences among the various models. For ATD and AMD the DFT/MM calculations predict blueshifts of only about 20 cm^{-1}, for ATD* and BMD blueshifts of more than 50 cm^{-1}, and for SML even a 22 cm^{-1} redshift. With a few exceptions the remaining stretching modes show minor and varying frequency shifts upon transfer of an oxidized flavin from TIP3P water into the rMD equlibrated BLUF models.

For the depicted frequencies the rmsd from the reference spectrum T3 is smallest at SML (19.8 cm^{-1}), slightly larger at AMD (20.0 cm^{-1}), at ATD (23.2 cm^{-1}), and at BMD (28.6 cm^{-1}). However, at ATD* the rmsd is exceptionally large as it measures as much as 45.4 cm^{-1}. All these RMSDs (see Table S2 in the SI) exceed the expected deviations of at most 10 cm^{-1} by at least a factor of 2, where we have based this accuracy expectation on previous experiences with DFT/MM descriptions of condensed phase IR spectra.[8,14] Despite our care in transforming the experimental structures into all-atom simulation models, certain aspects of these models must be grossly erroneous.

This conclusion is valid even if one doubts whether the quite large[19,64] DFT/MM frequency scaling factor of 1.031 is actually transferable from TIP3P water to CHARMM22 protein models. A CHARMM22 adapted and most likely smaller scaling factor will solely introduce a homogeneous compression of the frequency spectra and, therefore, cannot heal the strikingly different computational results shown in Figure 3 for models of several BLUF domains (AppA, BlrB, and Slr1694), whose chromophores have very similar vibrational spectra.[34−38] Thus disregarding the open question on the transferability of the DFT/MM frequency scaling factor, there remain several possible sources for the apparent misdescriptions. These error sources may vary among the various existing structural models and, therefore, will be discussed by sequentially considering the various structures.

In this context we will present several computer experiments, in which the electrostatics of BLUF residues featuring hydrogen bonds (H-bonds) with the C═O groups of the FMN chromophore are specifically modified. These computer experiments serve to reveal the mechanisms, by which a BLUF protein can steer the frequencies of FMN's important C═O stretching modes.

Why BLUF Structures Do Not Fit to Vibrational Spectra. *NMR Model ATD**. We start the discussion with the NMR structure ATD*,[25] because this model shows the exceptionally large rmsd of 45.4 cm^{-1} from the T3 reference. According to Figure 3 this rmsd is mainly due to enormous blueshifts of the two C═O stretching frequencies. Figure 3 furthermore demonstrates that the spectrum calculated for ATD* shows substantial deviations (rmsd: 29.3 cm^{-1}) also from the spectrum calculated for the X-ray structure ATD[21] of the same BLUF domain in the same conformation. The large RMSDs, by which the spectrum calculated for the solution NMR structure ATD* deviates from the T3 reference and from the spectrum obtained for the crystal X-ray structure ATD, require an explanation.

An obvious difference between ATD* and ATD is that ATD* is provided in the PDB as a monomer (2BUN) instead of a dimer. Like ATD (1YRX) also the X-ray structure AMD[39] (2IYG) of the same BLUF domain in the other (Met_{in}) conformation is a dimer. To check whether the monomeric modeling causes the much larger rmsd of ATD*, we additionally calculated the IR frequencies for FMN in a solvated AMD monomer. However, the spectra of the AMD monomer and dimer turned out to differ by a rmsd of only 7.2 cm^{-1} (data not shown). Furthermore the spectra of the AMD and ATD dimers differ only by an rmsd of 6.7 cm^{-1}. Therefore, the monomeric character of ATD* cannot be the cause for its much too large RMSDs of 29.3 cm^{-1} from the ATD and of 45.4 cm^{-1} from the T3 references.

Another reason for the huge 45.4 cm^{-1} rmsd observed for ATD* could be the assumption that His44 is deprotonated (cf. our remark in Methods on an apparent contradiction in ref

25 concerning this issue). However, the protonation of His44 does not reduce the rmsd of ATD* very much. It is still 40.6 cm^{-1} (cf. Table S2 in the SI) and, thus, by far too large. In the case of the other AppA BLUF models ATD and AMD the protonation even increases the associated RMSDs a little (Table S2), which is the reason why we omitted the DFT/MM spectra calculated for ATDP and AMDP in Figure 3. However, for the sake of completeness the shifts introduced by the protonation of His44 in the DFT/MM vibrational spectra of the various AppA BLUF models are illustrated by Figure S12 in the SI.

The facts that for ATD* the rmsd from the T3 reference is about two times larger than for ATD and that, consequently, ATD* deviates by a large rmsd from ATD, must be caused by substantial structural differences between the underlying experimental models, although they should map one and the same protein conformation. Ideally, ATD* should represent the structure of AppA BLUF in solution and, hence, should belong to conditions silimar to those used in vibrational spectroscopy, whereas ATD might be modified by crystal artifacts.

Figure S13 in the SI demonstrates that ATD and ATD* actually assign drastically different structures to the FMN binding pocket of AppA BLUF (Trp_{in} conformation). The associated quite detailed discussion explains the differences between the spectra calculated for ATD and ATD* as consequences of different protein-chromophore interactions, which are associated with different local structures. In particular, the discussion argues that the missing H-bond FMN−O4···H−N−Asn45 in the NMR structure ATD* must lead to strongly blueshifted C═O stretching frequencies as seen in Figure 3. FMN−O4 is strongly H-bonded in water[41] and in other AppA BLUF structures (cf. Figure 1, panels a and b, and Figure S11 in the SI), which therefore feature red-shifted C═O stretches. The discussion in the SI concludes that the NMR structure ATD* with its hardly H-bonded FMN-O4 is incompatible with the observed vibrational spectra.

The much smaller rmsd calculated by us for ATD as compared to ATD* now argues that ATD as depicted in Figure 1a is closer to the AppA BLUF structure present and observed in vibrational spectroscopy than ATD*. Because we want to analyze these spectra, we have excluded the obviously error-prone NMR structure ATD* from further considerations.

X-ray Model SML. According to Figure 3 the spectrum calculated for the X-ray model SML[24] exhibits an unusually red-shifted $[C2{=}O]_-$ stretching frequency. Not even in TIP3P water, where FMN-O2 is quite strongly H-bonded to the surrounding solvent,[41] the H-bonding interactions manage to shift the $[C2{=}O]_-$ stretch below the $[C{-}C]_{RI}$ stretching vibration of FMN's ring I [cf. Figure 1(c)]. In SML there must be a very special structural reason for the unusually low $[C2{=}O]_-$ stretching frequency.

If one now looks at the structure of SML depicted in Figure 4 and compares this structure with those of the other BLUF domains in Figures 1a,b and 5, one actually detects a unique feature. Only in SML a charged residue (Arg68) forms an additional H-bond with the atom FMN-O2. In the other BLUF domains the charged Arg68 of Slr1694 is replaced by the polar His78 (AppA) or by the unpolar Leu66 (BlrB), which are located at the protein surfaces. Looking at the crystal structure of SML in a representation highlighting the protein surface (picture not shown) one recognizes that the side chain of Arg68 is buried with its charged tip in the protein interior where it forms the H-bond with FMN-O2 shown in Figure 4, top. This special structure

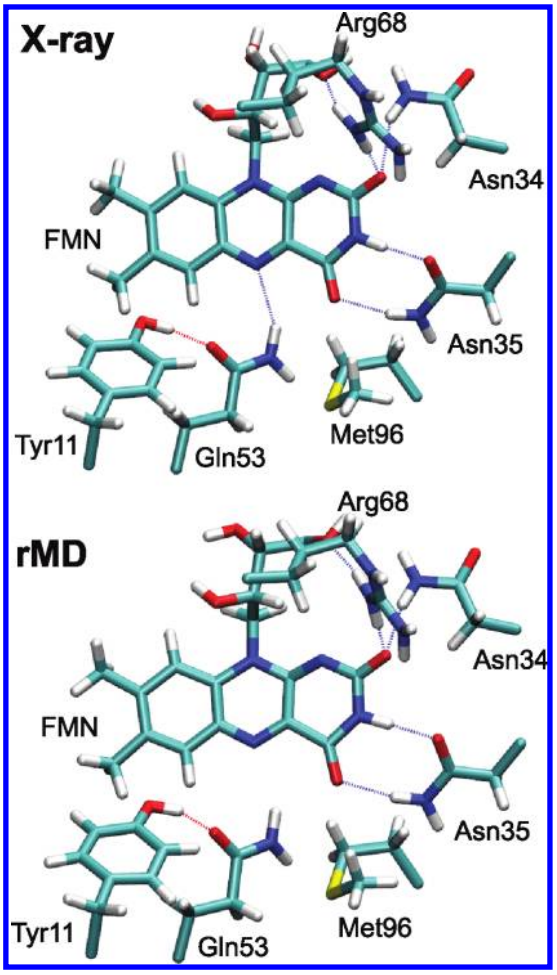

Figure 4. Comparison of the Slr1694[24] X-ray structure (top) with the best matching representative SML (bottom) in the rMD equilibrated structural ensemble. Quite obviously the X-ray structure is closely preserved by the rMD representative apart from the formation of somewhat tighter H-bonds. Furthermore the H-bonding pattern connecting FMN with Asn35, Gln53, and Tyr11 closely resembles the corresponding pattern in AMD [cf. Figure 1b].

immediately explains the 20 cm^{-1} redshift of the $[C2{=}O]_-$ stretching frequency calculated for SML as compared to T3.

To check this simple explanation we carried out a computer experiment. Here, we repeated the DFT/MM calculation of FMN's vibrational spectrum for a model SML* differing from SML solely in the partial charges of the Arg68 side chain. All of these partial charges were reduced by a factor 1/4 thus transforming Arg68 into an essentially unpolar residue. With the unpolar "Arg68" the $[C2{=}O]_-$ stretching frequency experienced a huge 79 cm^{-1} blueshift toward 1716 cm^{-1}, whereas all other FMN stretching frequencies showed much smaller shifts of about 10 cm^{-1}. As a result, the upshifted $[C2{=}O]_-$ frequency was close to the value of 1710 cm^{-1} calculated for BMD, in which FMN-O2 is lacking a clear H-bond (see below), and far above ($\sim$36 cm^{-1}) the frequencies found for ATD and AMD, where FMN-O2 forms a H-bond with a water molecule that has entered the protein during the rMD equilibrations [cf. Figure 1, panels a and b].

Spectroscopically, however, the $[C2{=}O]_-$ band of flavin is found at the same frequency of 1670 cm^{-1} both for solubilized

dark-adapted Slr1694[34,37] and for aqueous solution[45−49] demonstrating that the H-bond between FMN-O2 and Arg68 must be absent in the solubilized protein Slr1694 studied by vibrational spectroscopy. Instead one must expect that the ionic side chain of Arg68 becomes solvent exposed in the solvated protein. Here, FMN-O2 may either form a slightly stronger H-bond with Asn34 (cf. Figure 4) or with water molecules entering the protein and replacing Arg68, which both could explain the observed spectral position of the [C2═O]_ band.

Our calculations definitely exclude, however, the extremely strong H-bond of FMN-O2 with Arg68 for solubilized Slr1694, because that would argue for a [C2═O]_ frequency near 1630 cm^{-1}. For this estimate we took the 40 cm^{-1} shift, by which the extremely strong H-bond of FMN-O2 with Arg68 in SML shifts the [C2═O]_ frequency to the red of the 1680 cm^{-1} calculated for the moderatly strong H-bonds of FMN-O2 in ATD and AMD (cf. Figure 3). This estimate is valid because the structures of SML and AMD are very similar in many respects with the key exception of the H-bonding at FMN-O2.

Thus, we conclude that the H-bond between FMN-O2 and the charged tip of Arg68 is an artifact of the SML crystal, which is caused by a reduced polarity of the Arg68 environment within the crystal lattice and will disappear upon solvation of the protein in aqueous solution. Therefore, the X-ray structure of SML is inappropriate for comparisons of calculations with observed solution spectra, which is the reason why we have excluded it from further considerations.

We would like to note that the soft restraints on the heavy atoms applied in our rMD simulations were strong enough to preserve the electrostatically unfavorable buried position of Arg68 present in the low-dielectric crystalline environment. We expect, however, that extended and unrestrained MD simulations with a sufficiently accurate MM force field will produce solution structures of SML featuring a solvent exposed Arg68, which then could qualify for DFT/MM calculations of the vibrational spectra.

X-ray Model BMD. Similar to the case of SML just discussed also the spectrum calculated for the X-ray model BMD[52] shows an unexpected feature. But instead of an unusual redshift of the [C2═O]_ stretch frequency one here notes an unusual blueshift of that frequency. Figure 3 shows that this frequency is calculated 51 cm^{-1} above the T3 reference and about 30 cm^{-1} above the [C2═O]_ frequency obtained for the AppA BLUF models ATD and AMD. Following the arguments given above concerning the influence of H-bonds at FMN-O2 on the [C2═O]_ frequency, we are led to conclude that sufficiently strong H-bonds resembling those found in liquid water must be absent in the X-ray structure of BlrB.[52]

In fact, if one looks at the X-ray structure and at the structure of its best matching rMD representative BMD depicted in Figure 5, one sees that FMN-O2 has no H-bonding partner. In BMD the His44 side chain in AppA BLUF is replaced by the longer side chain of Arg32, which in the crystal forms H-bonds with the phosphate group of FMN's ribityl-5′-phosphate side chain. Our rMD equilibration preserves this structural arrangement, which prevents the approach of water molecules from the surrounding solvent toward FMN-O2 and the formation of H-bonds like in the rMD models of ATD and AMD [cf. Figure 1, panels a and b]. In an extended unrestrained simulation with a sufficiently accurate MM force field, however, as well as in a solution structure one should expect that the zwitterionic structure, which is present in the crystal and consists of the phosphate and Arg32,

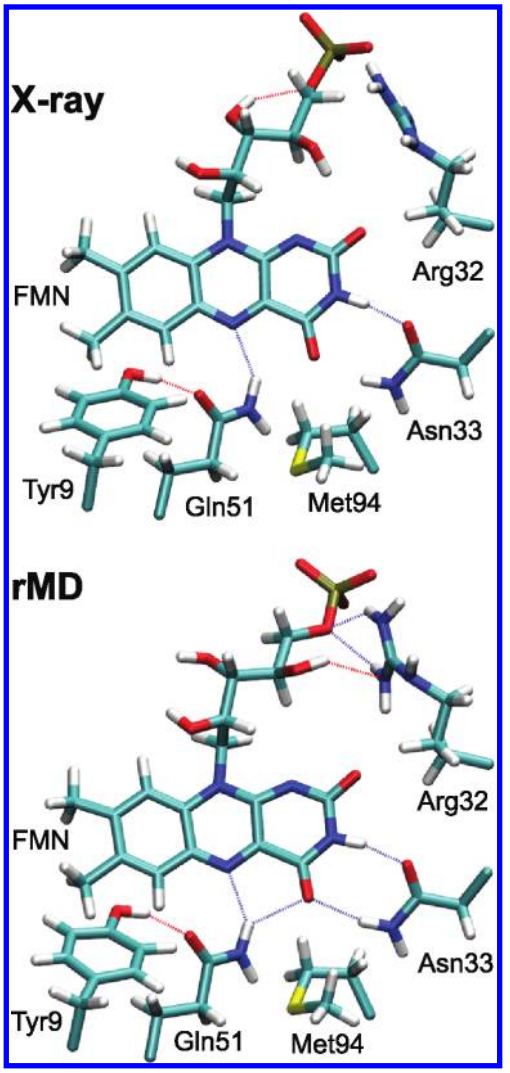

Figure 5. Comparison of the BlrB[52] X-ray structure (top) with the best matching representative BMD (bottom) in the rMD equilibrated structural ensemble. The two structures are highly similar and resemble those of AMD in Figure 1b and of SML in Figure 4, if one disregards the obvious replacements of Arg32 by His44 (AMD) and Asn34/Arg68 (SML) near FMN-O2 as well as the additional water molecule generated by the rMD equilibration in AMD.

is unstable, because both ions should prefer to become solvated in the adjacent aqueous phase. Such a solvated structure will then show H-bonds between water molecules of the solvent and FMN-O2, which can easily reduce the [C2═O]_ frequency by about 30 cm^{-1}.

Because of the lacking H-bonds at FMN-O2 and of the associated artificial blueshift of the [C2═O]_ frequency also the X-ray structure of BlrB[52] and its rMD model BMD cannot serve as computational tools to describe the vibrational spectra[34−38] of FMN embedded in solvated BLUF domains. The spectral positions of the C═O stretching bands in these spectra are close to those in water and, therefore, clearly signify strong H-bonds at FMN-O2 and FMN-O4.

Although the X-ray structure of BlrB may possibly reflect the reality of the crystal, it nevertheless may not represent the solution structure of this BLUF domain, because a lacking H-bond at FMN-O2 should leave clear footprints also in the

optical spectra of the chromophore, which have not been observed, however.[52] Whether a mobile water molecule, which could be present in the BlrB crystal, has been overlooked during refinement could be decided, if in addition to X-ray data also chromophore vibrational spectra would have been recorded for the crystals. Similarly, whether FMN-O2 is H-bonded, if BlrB is solvated in water, could be decided by corresponding IR spectra. Because of the lacking data on the chromophore vibrational spectra of BlrB both in the crystal and in solution we have to exclude the model BMD from further analysis.

Intermediate Summary and Discussion. The above analysis employed rMD simulations of various structural models for BLUF domains and first DFT/MM computations of the FMN vibrational spectra with the aim to check, whether these experimentally derived models qualify for explanations of FMN's vibrational spectra that were recorded for solubilized BLUF domains.

Luckily we found the two structural models ATD and AMD, which passed our initial test. We note in passing that these structures would not have passed this test either, if the rMD equilibration had not placed a H-bonded water molecule close to the atom FMN-O2 [cf. Figure 1, panels a and b], which is missing in the crystal structures. The reason for the expected failure is that a H-bonding strength similar to that in aqueous solution is necessary to move the $[C2{=}O]_-$ frequency from non-H-bonded values[41] above 1740 cm^{-1} toward a value (1670 cm^{-1}) similar to the one found in water.

Other X-ray models either lacked such a H-bond at FMN-O2 (BMD), because the X-ray structure does not contain a water molecule at the required location and because the rMD simulation did not manage to heal this likely error, or showed a much too strong H-bond at FMN-O2 (SML), because in the crystal an arginine side chain preferred to become buried in the protein interior instead of becoming solvated in the surrounding solvent. For these crystals a knowledge of FMN's vibrational spectra could lead to immediate checks of the correctness of the X-ray structures. In both cases the solution structures will most likely differ from the respective crystal structures, because charged residues at the protein surfaces will become solvated. Then, both solution structures will closely resemble the structure AMD shown in Figure 1b.

Despite the thus established structural similarity of the solubilized BLUF proteins AMD, BMD, and SML, two of these Met_{in} structures (AMD and BMD) were interestingly associated with the dark-adapted resting state,[39,52] whereas one (SML) was assigned to the light-adapted signaling state.[24] The latter assignment was based on the quenching of the Trp fluorescence after light excitation of Slr1694 BLUF and the empirical rule that polar solvents tend to quench this fluorescence.

For the NMR structure ATD* a spectral comparison with the X-ray structure ATD clearly revealed gross inaccuracies of atomic coordinates, which excluded this model from further analysis. Finally, the X-ray structure AML (chain A in the PDB entry 2IYI[39]) did not even pass the test of dynamical stability. Upon the rMD equilibrations it decayed toward a structure resembling that of AMD. On the other hand, the model AML_B derived from chain B of 2IYI was dynamically stable but featured a H-bonded network so similar to that of AMD that the C=O stretching frequencies calculated for AMD and AML_B deviated by at most 1 cm^{-1}, which is why the choice of structure AMD seemed to be sufficient for the further characterization of the Met_{in} conformation of AppA BLUF.

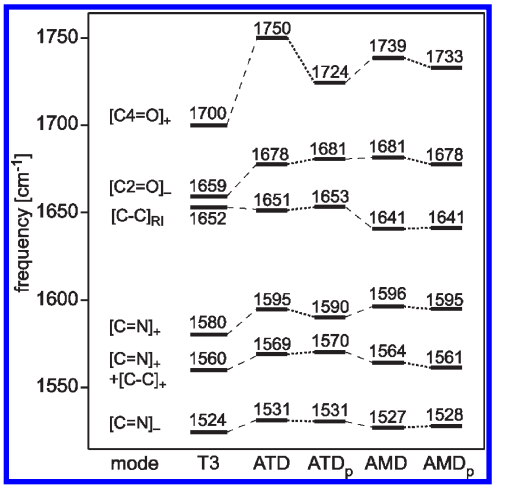

Figure 6. Polarization effects on the scaled DFT/MM vibrational frequencies calculated for FMN in the rMD equilibrated BLUF models ATD and AMD. The effects are due to replacing in the FMN binding pockets the standard partial charges of CHARMM22[15] with the self-consistent ESP charges of the respective structure adapted PFFs (subscript "p") derived from iterative DFT/MM calculations (see the text and the SI for details). Also given is the reference spectrum T3.[41]

X-ray Models ATD and AMD. As a result, we are left with the models ATD and AMD drawn in Figure 1, panels a and b, and with their descendants ATDP and AMDP distinguished by a protonated His44. As we pointed out above in our discussion of Figure 3 and Table S2 in the SI, also for these models the DFT/MM spectra of the FMN chromophore calculated at the respective best matching rMD equilibrated structures show RMSDs from the T3 reference spectrum exceeding the expected value[14] of 10 cm^{-1} by a factor of 2.

Following the arguments of Babitzki et al.,[19] a possible reason for the unexpectedly large RMSDs obtained for these AppA BLUF models could be the use of the standard MM force field CHARMM22 for the description of the BLUF proteins surrounding the DFT fragment, i.e., the flavin chromophore. The neglect of the electronic polarizability is inherent to such a standard MM force field and could lead to an ill-structured electrostatic potential within the FMN binding pocket, which could be witnessed, e.g., by an insufficiently stable H-bonded network. To check this issue, we calculated for the binding pockets of the four rMD equilibrated AppA BLUF models new ESP[76] partial charges by the iterative DFT/MM procedure outlined in Methods. The resulting structure adapted partial charges are listed in Tables S3−S13 of the SI, and the corresponding PFFs were used to recalculate the IR spectra of FMN in the AppA BLUF models ATD and AMD.

Polarization Effects on the IR Spectra of FMN in AppA BLUF. Figure 6 illustrates the spectral changes which are induced, if one replaces the CHARMM22 force field by the respective structure adapted PFFs in the rMD equilibrated simulation models ATD and AMD. For both models the $[C4{=}O]_+$ frequency is seen to be red-shifted upon exchanging in the rMD equilibrated models the standard CHARMM22 partial charges by those of the structure adapted PFFs. The frequencies of the other FMN stretching modes show only minor changes.

As a result the rmsd from the T3 reference spectrum decreases by 23% for ATD_p and by 19% for AMD_p. Thus, accounting for

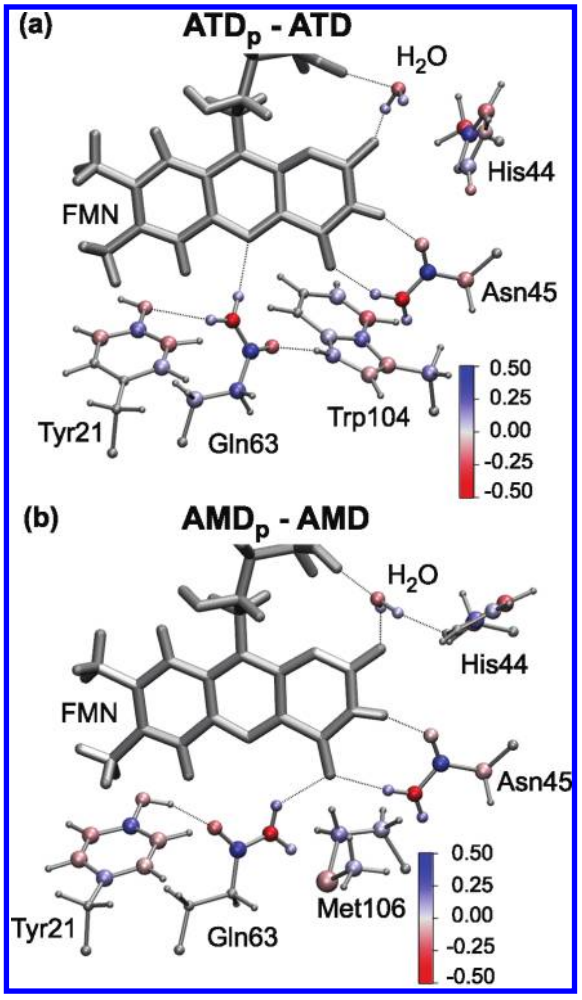

Figure 7. DFT/MM derived differences $\Delta q_i = q_i(p) - q_i(c)$ between the atomic partial charges q_i characterizing the PFF models $p \in \{ATD_p, AMD_p\}$ and the CHARMM22 models $c \in \{ATD, AMD\}$. Negative Δq_i are colored in red and positive Δq_i in blue.

the electronic polarization somewhat reduces the unexpectedly large RMSDs calculated with CHARMM22 (cf. Tables S2 and S14 in the SI). To identify the reasons, why the DFT/MM spectra of the models ATD_p and AMD_p are closer to the T3 reference, we consider the changes of the charge distributions induced by the polarization of the FMN binding pocket in AppA BLUF.

Polarization of the FMN Binding Pocket in AppA BLUF. Figure 7 partially illustrates the polarization effects Δq_i on the partial charges q_i in the FMN binding pockets of (a) ATD and (b) AMD (effects omitted in the drawings are documented by Tables S3−S13 in the SI). For both models one immediately recognizes that the electronic polarization makes the C═O and NH_2 groups of Asn45 and Gln63 much more polar than assumed by CHARMM22. In particular, the H-bonds FMN−O4···H−N−Asn45 and FMN−N3−H···O−Asn45 become stronger by 44% and 18%, respectively, upon inclusion of the electronic polarizability. Interestingly also the strongly bound water molecule, which forms a H-bond with FMN-O2, becomes more polar. Its dipole moment is in both PFFs by about 20% larger than assumed by TIP3P (cf. ref 18).

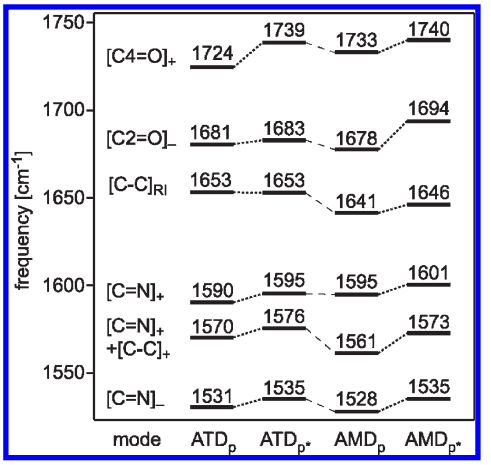

Figure 8. Vibrational frequencies calculated by DFT/MM for FMN embedded in the BLUF models ATD_p and AMD_p are compared with those of ATD_{p^*} and AMD_{p^*}, respectively, whose PFF were modified by adopting for Asn45 the less polar CHARMM22 model instead of the highly polar Asn45 model calculated by DFT/MM.

Spectral Role of the Asn45 Polarity in AppA BLUF. The strongly increased polarity of Asn45 in the two polarized AppA BLUF models should be the cause for the polarization-induced redshifts of the $[C4{=}O]_+$ frequency shown in Figure 6. To check this issue we carried out another computer experiment. Here, we repeated the calculation of the vibrational spectra for modified PFF models ATD_{p^*} and AMD_{p^*} of AppA BLUF, in which solely the highly polar residue Asn45 resulting from the DFT/MM calculations was replaced by its much less polar CHARMM22 model (cf. Table S6 in the SI).

Inspection of Figure 8 immediately shows that the decreased polarity of Asn45 entails a blueshift of essentially all FMN stretching frequencies. In particular, this polarity reduction shifts the average C═O stretching frequency, which we define as $\bar{\nu}_{C=O} \equiv (\nu_{C4=O} + \nu_{C2=O})/2$, by 9 and 12 cm^{-1} to the blue as compared to ATD_p and AMD_p, respectively. Because the polarities of many residues in the FMN binding pocket were changed during the iterative DFT/MM calculations of the PFFs (cf. Figure 7 and Tables S3−S13 in the SI), the partial restoration of the CHARMM22 force field at Asn45 does not lead back to the CHARMM22/DFT spectra ATD and AMD of Figure 6. In the case of the $[C4{=}O]_+$ frequency of ATD, for instance, the PFF polarity of Asn45 explains only 58% of the 26 cm^{-1} redshift calculated for the transition toward the PFF model ATD_p. As a rule of thumb we may nevertheless state that the strength of the H-bond FMN−O4···H−N−Asn45 as given by the polarity of Asn45 in our DFT/MM setting steers the spectral position of the average C═O stretching frequency $\bar{\nu}_{C=O}$ in general and of the $[C4{=}O]_+$ frequency in particular. Thus, the common explanation that the 17 cm^{-1} redshift of the $[C4{=}O]_+$ frequency observed in the dark-light transition of BLUF domains[34−38] signifies an increased H-bonding strength at FMN-O4, is clearly supported by our second computer experiment.

We would like to stress at this point that the three structures ATD, ATD_p, and ATD_{p^*} obtained by DFT/MM minimization from the associated rMD equilibrated model are nearly identical as we have checked by graphical inspection. A likewise striking structural similarity implying movements of FMN atoms of the order of only 0.05 Å holds for the DFT/MM optimized structures AMD, AMD_p, and AMD_{p^*}. Therefore, the spectral

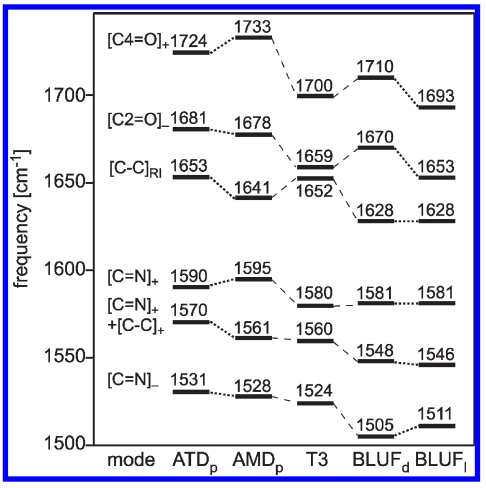

Figure 9. Frequencies calculated by DFT/MM for oxidized flavin in the ATD_p and AMD_p models of AppA BLUF and in the TIP3P model of liquid water (T3), which were scaled by 1.031, are compared with experimental consensus frequencies[34−38] for flavin in the dark ($BLUF_d$) and light ($BLUF_l$) states of BLUF domains.

shifts seen in Figures 6 and 8 among the various spectra for ATD and AMD, respectively, are almost exclusively caused by the differences among the partial charges used to model the electrostatics of the protein environments.

Together with the results of our calculations on SML and BMD, which showed that the $[C2{=}O]_-$ frequency can be selectively tuned by H-bonding interactions at FMN-O2, the picture emerges that the frequencies of FMN's important C═O stretches are mainly steered by the strengths of local H-bonds. These simple rules agree, of course, with the results of our previous calculations on LF in water[41] and with expectations common[34−36] among spectroscopists.

Transferability of Frequency Scaling. As we have seen, the use of PFFs for the AppA BLUF models ATD and AMD has shifted the C═O stretching frequencies toward the desired values. Unfortunately, the H-bonding interaction of FMN with the highly polar Asn45 provided by the PFFs did not suffice to bring the average C═O frequency $\overline{\nu}_{C=O}$ of 1698 (ATD_p) and of 1706 cm^{-1} (AMD_p) down to the value of 1680 cm^{-1} predicted by the reference calculation T3 or to the somewhat larger value of 1690 cm^{-1} observed[34−38] for dark-adapted BLUF domains.

To illustrate this issue we now compare the scaled (1.031) DFT/MM frequencies with spectroscopic data on BLUF domains. We extracted these data as averages from available IR and RR spectra on flavins in the dark- and light-adapted states of BLUF domains in Slr1694[34,37] and AppA.[35,36,38] Here, we cannot exclusively rely on spectra for AppA, because the $[C2{=}O]_-$ frequency has not been determined for this protein. On the other hand, the spectra for AppA and Slr1694 are very similar for the remaining bands.

Figure 9 demonstrates that the vibrational frequencies calculated for FMN in the rMD equilibrated AppA BLUF models ATD_p and AMD_p are strongly and about homogeneously blueshifted compared to the experimental data represented in the columns $BLUF_d$ and $BLUF_l$. In contrast, the LF spectrum T3, which is calculated with the TIP3P model of an aqueous solution, covers about the same spectral range as the experimental $BLUF_d$ reference spectrum, which closely resembles the vibrational spectrum observed for oxidized LF in aqueous solution (data not shown).[41]

Note, however, that the two C═O frequencies in column T3 of Figure 9 are red-shifted compared to the experimental $BLUF_d$ reference, whereas many of the other frequencies show sizable blueshifts. This indicates that the TIP3P scaling factor of 1.031 does not quite succeed to shift the C═O frequencies, which are extremely sensitive to the strengths of local H-bonds,[41] to sufficiently large values, while it shifts most other frequencies, which are less sensitive to H-bonding, too far to the blue. The stated imbalance of scaling-induced frequency shifts shows that a TIP3P environment considerably overestimates the H-bonding strength of real water. With a smaller scaling factor many T3 frequencies would match the observations much better, but the H-bonding sensitive C═O frequencies would then represent gross underestimates. We note that the stated overstimate of the H-bonding strength by the TIP3P water model leads to a dielectric constant,[77−79] which is by about 25% larger than that of real water.

The nearly homogeneous overestimates of the experimental data in columns $BLUF_d$ and $BLUF_l$ of Figure 9 by the computational results in columns ATD_p and AMD_p demonstrate that the application of the large TIP3P scaling factor is inappropriate and that a smaller factor must be chosen. Thus, our initial assumption that the TIP3P adjusted scaling factor of 1.031 should be transferable to CHARMM22 or PFF models for protein environments was incorrect. This conclusion is supported by earlier DFT/MM descriptions of chromophore vibrational spectra,[19,64] which also combined the MT/BP approach with CHARMM22 or PFF models of the respective protein environments but used much smaller scaling factors of 1.0122 and 1.005, respectively. We note that the assumption of a protonated His44 in AppA BLUF does not change this conclusion. On the contrary, as documented in the SI by Figures S14 and S15 and as explained in the accompanying text, the protonated models describe the experimental spectra generally even worse than the unprotonated models (cf. Table S14).

DFT/MM Results for FMN in ATD and AMD. To compute a scaling factor, which is more appropriate for the DFT/MM description of FMN in PFF models of BLUF domains, we have matched the spectra ATD_p and AMD_p to the spectra $BLUF_d$ and $BLUF_l$ by minimizing the total rmsd for all pairwise comparisons. This procedure was chosen, because we did not want introduce a prejudice for the assignment of ATD_p and AMD_p to the dark or light states of BLUF domains. We found the strongly reduced scaling factor of 1.0187. It entails RMSDs of 7.2 and 6.6 cm^{-1} matching ATD_p and AMD_p, respectively, to $BLUF_d$. For the light state spectrum $BLUF_l$ the corresponding deviations are 7.6 (ATD_p) and 8.7 cm^{-1} (AMD_p) (cf. Table S15 in the SI). Because of the slightly better matches with the dark state spectrum $BLUF_d$ it may seem that both AppA conformations, i.e., Trp_{in} (ATD_p) and Met_{in} (AMD_p), represent the dark state.

Figure 10 illustrates the quality, at which the properly rescaled vibrational frequencies, which were calculated by DFT/MM for FMN in the rMD equilibrated AppA BLUF models ATD_p and AMD_p, explain the spectroscopic data[34−38] on the dark- and light-adapted states of BLUF domains, respectively. As already indicated by the RMSDs, the frequencies calculated for ATD_p and AMD_p are seen to fit better to the experimental dark state frequencies $BLUF_d$. Most of the dark state frequencies are close or nearly identical to those measured for the light state ($BLUF_l$) with the important exceptions of the two C═O frequencies, which are both red-shifted by 17 cm^{-1}. According to the

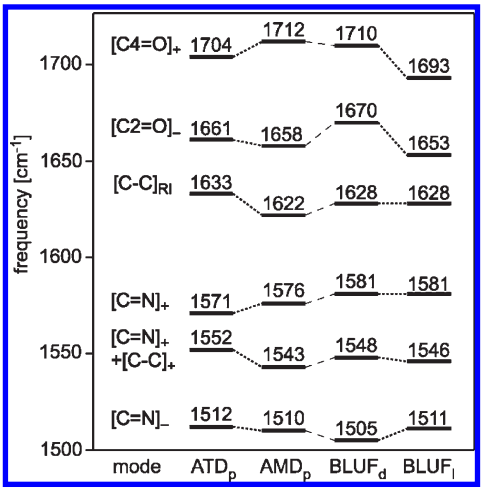

Figure 10. Vibrational frequencies, which were calculated by DFT/MM for FMN in the BLUF models ATD_p and AMD_p, are compared after application of the new scaling factor 1.0187 with spectroscopic data[34−38] on the dark ($BLUF_d$) and light ($BLUF_l$) states of BLUF domains.

computational results presented further above, these redshifts indicate that the H-bonding interactions at FMN-O4 and FMN-O2 must be stronger in the light than in the dark state. In contrast, the calculated spectra depicted in Figure 10 for ATD_p and AMD_p do not reveal clearly stronger H-bonds at FMN's carbonyl groups in one of these structures suggesting again that both models belong to the dark state.

Can We Assign Conformations to Functional States? At this point readers interested in a clear-cut assignment of the experimentally known BLUF structures to one of the two functional states of BLUF domains, i.e., the dark-adapted resting and the light-adapted signaling state, respectively, may ask to what extent the above conclusion that both conformations Trp_{in} (ATD_p) and Met_{in} (AMD_p or AML_{Bp}) belong to the dark state is actually solid. Here, we have to admit that we are quite uncertain concerning a certain part of this question, i.e., the one concerning the Met_{in} conformation, and we will now give arguments why this uncertainty cannot be avoided because of insufficient statistics.

First, our above analysis has been based solely on single though hopefully representative structures. However, our previous study on LF in TIP3P water has shown that thermal fluctuations of the H-bonds cause large fluctuations (∼15 cm^{-1}) of the C═O frequencies.[41] Correspondingly, other structural snapshots from the rMD equilibrated ensemble could have given somewhat different spectra fitting to different assignments.

If one assumes, for instance, that the $[C4{=}O]_+$ frequency of AMD_p would have been calculated at 1702 cm^{-1} instead of 1712 cm^{-1}, the rmsd from the experimental dark state spectrum $BLUF_d$ would increase from 6.6 to 7.3 cm^{-1} and the rmsd from $BLUF_l$ decrease from 8.1 to 5.4 cm^{-1}. These RMSDs would then indicate that the Met_{in} conformation AMD belongs to the light state and not to the dark state.

Furthermore, one can easily imagine conditions, which could bring about such a 10 cm^{-1} redshift of the $[C4{=}O]_+$ frequency. According to the computer experiment documented by Figure 8 it can be caused by H-bonding interactions at FMN-O4, which are somewhat stronger than those present in the DFT/MM optimized structure AMD_p. In fact, the DFT/MM optimized structure of $AMDP_p$, in which His44 is protonated, shows stronger H-bonds at FMN-O4. Thus, the $[C4{=}O]_+$ frequency is by 8 cm^{-1} smaller than in AMD_p (cf. Figures S16 and S17, Table S16, and the associated text in the SI). It may well be that similarly strong H-bonds can be found for many other snapshots of AMD's rMD ensemble. Then this Met_{in} ensemble would be classified as "light state".

Finally, it could even be that an additional water molecule, which has not been identified in the X-ray structures of the Met_{in} conformers allegedly representing the light state (e.g., SML or AML_B) is H-bonded to FMN-O4 in that state. If this should be the case, the 17 cm^{-1} red shift observed in the dark-light transition might be explained. But then none of the experimental structures studied by us would comply with the light state vibrational spectrum and all of them would have to be classified as belonging to the dark state.

As a check we carried out a computer experiment, in which we added to the model AML_{Bp} a TIP3P water molecule H-bonded to FMN-O4, because AML_B as opposed to AMD features a cavity near the FMN due to a movement of Met106.[39] This water molecule stayed attached to FMN-O4 during 150 ps of rMD simulation. We found by DFT/MM for an arbitrary snapshot that the C═O frequencies experienced an average red shift of 8 cm^{-1}. As a result the computed spectrum resembled more closely the experimental $BLUF_l$ data than the $BLUF_d$ data. However, like the spectra of unperturbed AMD_p, AML_{Bp}, and ATD_p also this modeling effect needs an extended statistics for a precise DFT/MM characterization within the INMA approach.

As a result we see that the missing large scale statistics over the rMD snapshot ensembles is the reason, why we cannot surely assign the Met_{in} conformation to the light or to the dark state of AppA BLUF. In contrast, the Trp_{in} structure does not provide any chance for stronger H-bonds at FMN-O4 and, therefore, belongs quite surely to the "dark state". Here, the snapshot chosen for the computation of the PFF even happened to render a somewhat too strongly polar residue Asn45. In fact, we have checked that 85% of the snapshots in the rMD equilibrated ATD ensemble yield less polar H_2N-Asn45 groups. Referring again to the computer experiment illustrated by Figure 8, a reduced polarity would entail for ATD a further blueshift of the $[C4{=}O]_+$ frequency well fitting to $BLUF_d$.

Note that the still possible assignment of the Met_{in} conformation to the light state and the quite certain association of the Trp_{in} conformation to the dark state of BLUF domains explained above agree with interpretations of the altered Trp fluorescence quenching upon light-adaptation[24] and with other experimentally derived arguments.[21,22,25,26,80,81]

Sufficient Statistics? The above DFT/MM analysis of the BLUF chromophore vibrational spectra was carried out in a classical quantum chemistry style by considering single albeit carefully chosen structures instead of thermalized structural ensembles, which are much more appropriate, if one wants to compute room temperature properties of soft-condensed matter. An ensemble approach has been used by us in our preparatory DFT/MM work on the IR spectra of flavins in solution.[8,41] Correspondingly, we obtained estimates on the widths and shapes of the various flavin IR bands, which are inaccessible in the single snapshot scenario employed in the work presented above.

In the given case the desirable ensemble approach posed an effort, which was unmanageable with the means presently available to us. Within such an approach one should compute

ensemble average PFFs by DFT/MM in a self-consistent manner for all considered BLUF models instead of computing just single PFFs for selected snapshots. Here, self-consistency requires to recalculate the rMD equilibrated ensembles iteratively with ensemble average PFFs until they become stationary. Given completely automated procedures for all required computational steps and large computational resources such a task will become manageable. To us it was precluded, because only parts of the procedures could be automated in the present project and because our computational resources were too small.

Correspondingly, the second step, which would have been the DFT/MM computation of vibrational spectra for thermal snapshot ensembles by the INMA approach, remains to be tackled. Note that the INMA approach could be chosen in our preceding studies on the vibrational spectra of LF in solution,[8,41] because here only a few models for the environment had to be considered, whereas now we had to deal with seven BLUF models, with the unknown protonation state of His44 in AppA BLUF, and with the necessity to compute PFFs in addition to the standard CHARMM22 force field.

Because we considered only single structures, we could not surely decide whether the Met_{in} conformation as represented by the model AMD (or AML_B, which was not discussed in detail here) belongs to the light or to the dark state of AppA BLUF. For this reason we also cannot provide estimates on the statistical errors associated with our computational results. We have solely checked for selected amino acids like Asn45, how strongly its PFF varies within the given rMD equilibrated conformational ensemble, which then strengthened our assignment of ATD to the dark state. As a check for the validity of our speculative discussion on the structure of the dark and light states of BLUF domains we would have to know the ensemble average frequencies of the flavin C═O stretching vibrations instead of snapshot values. Unfortunately the lacking statistics on the PFFs and on the vibrational spectra has precluded a more reliable conclusions concerning the assignment of AMD (or possibly AML_B) to the dark or the light state of AppA BLUF.

Summary and Outlook. Despite the statistical uncertainties addressed above, certain results definitely prevail, because they reflect large, simple, and plausible electrostatic effects. Examples are the dynamical instability of the X-ray model AML[39] (cf. Figure 2 and Figure S11 in the SI), the apparent inaccuracy of the NMR structure ATD*,[25] or the steering of the $[C2{=}O]_-$ frequency by H-bonds at FMN-O2. This steering became apparent in the computations of vibrational spectra for the X-ray structures SML[24] of Slr1694 from the cyanobacterium *Synechocystis* and BMD[52] of BlrB from *Rb. Sphaeroides*. In these cases H-bonds, which are present (SML) or absent (BMD) in the crystals and are most likely absent (SML) or present (BMD) in the solution structures of these proteins, lead to the firm conclusion that the vibrational spectra calculated for the crystal structures are definitely incompatible with observed solution spectra. Also the steering of the average C═O frequency and, in particular, of the $[C4{=}O]_+$ frequency by H-bonding interactions at FMN-O4 is one of the unambigouos results, which supports well-known empirical rules.[34−36] Finally, the IR spectra calculated for the Trp_{in} conformation of AppA BLUF (ATD) fitted quite clearly to the spectroscopic data on the dark state, which agrees with previous assignments.[21,22,80]

Unfortunately, our lacking computational resources and the still incomplete automation of PFFs by iterative DFT/MM calculations and rMD equilibrations lead to statistical uncertainties, which precluded us to assign the Met_{in} conformation as represented by AMD or AML_B[39] definitely to the dark or light state of AppA BLUF. Based on our insights gained from the many calculations of FMN spectra for BLUF domains we nevertheless continue to speculate that the light state might feature a Met_{in} conformation.[26,81] It would be nice, if we had the means to substantiate our speculation better than we could do here.

Concerning the DFT/MM methodology our current study has underlined the necessity of a careful and cautious modeling in the conversion of X-ray structures into all-atom simulation systems. Using rMD equilibrations, which enable careful checks to what extent given experimental structures are compatible with force field descriptions, one can find out, whether these structures are trustworthy starting points for further computations. Based upon such a modeling, comparisons of vibrational spectra calculated for a crystal structure with spectra observed for solubilized proteins can provide clear evidence on conformational changes, which must occur upon transfer of the protein from the crystalline lattice into solution (see the cases of the BLUF domains Slr1694 and BlrB).

Furthermore, our investigation has emphasized the caveats resulting from an earlier study on the retinal chomophore of BR,[19] which state that the quality of standard nonpolarizable force fields is too poor for sufficiently accurate computations of protein chromophore vibrational spectra. By using PFFs calculated with DFT/MM techniques for BLUF domains the spectra computed for the FMN chromophore could be brought much closer to the observations.

The investigation has additionally shown that the electrostatics coded into the simple TIP3P model[70] for water is incompatible with the protein force field CHARMM22 or DFT/MM derived PFFs. Therefore, the frequency scaling factor (1.031) obtained from computing flavin vibrational spectra in TIP3P water[8,41] had to be reduced to 1.0187 to bring stretching frequencies calculated for FMN in BLUF domains described by PFFs close to observed values.

Finally our study rendered suggestions how one should include the effects of electronic polarization into the MM fragments of DFT/MM simulation systems. Here one may either choose a mean field approch by computing for a given protein conformation an ensemble average PFF or one may explicitly apply a polarizable MM force field. To make the mean field approach accessible, the lacking automated procedures should be generated and a faster DFT/MM approach should be used. The DFT program CPMD[60] used by us is definitely suboptimal for this purpose. More cost-effective calculations could become available through the program Quickstep,[82] for instance, once a suitable interface to a MM code like EGO[53] has been established. However, for a most cost-effective inclusion of the electronic polarization a new hybrid method combining the DFT description of a chromophore with a polarizable MM force field modeling its environment should be constructed and applied.

■ ASSOCIATED CONTENT

Supporting Information. Additional figures (S11−S17), tables (S2−S16), and various pieces of text explaining and documenting structural properties of the rMD equilibrated BLUF models, specifically for AppA BLUF domains the effects of His44 protonation on the chromophore vibrational spectra, the PFFs iteratively calculated by DFT/MM for the FMN

binding pockets of the rMD equilibrated AppA BLUF models, etc. This material is available free of charge via the Internet at http://pubs.acs.org.

AUTHOR INFORMATION

Corresponding Author

*E-mail: tavan@physik.uni-muenchen.de. Phone: +49 (0)89 2180 9220. Fax: +49 (0)89 2180 9202.

ACKNOWLEDGMENT

This work was supported by the Forschergruppe 526 "Sensory Blue Light Receptors" (DFG/FOR526) and by the Sonderforschungsbereich 749 "Dynamics and Intermediates of Molecular Transformations" (DFG/SFB749-C4) of the Deutsche Forschungsgemeinschaft.

REFERENCES

(1) van der Horst, M. A.; Hellingwerf, K. J. *Acc. Chem. Res.* **2004**, *37*, 13–20.
(2) Sancar, A. *Biochemistry* **1994**, *33*, 2–9.
(3) Ahmad, M.; Cashmore, A. *Nature* **1993**, *366*, 162–166.
(4) Christie, J. M.; Swartz, T. E.; Bogomolni, R. A.; Briggs, W. R. *Plant J.* **2002**, *32*, 205–500.
(5) Gomelsky, M.; Klug, G. *Trends Biochem. Sci.* **2002**, *27*, 497–500.
(6) Berg, J. M.; Tymoczko, J. L.; Stryer, L. *Biochemie*, 5th ed.; Spektrum Akademischer Verlag GmbH: Heidelberg, Germany, 2003.
(7) Siebert, F.; Hildebrandt, P. *Vibrational Spectroscopy in Life Science*; Wiley-VCH: Berlin, 2007.
(8) Rieff, B.; Bauer, S.; Mathias, G.; Tavan, P. *J. Phys. Chem. B* **2011**, *115*, 2117–2123.
(9) Eichinger, M.; Tavan, P.; Hutter, J.; Parrinello, M. *J. Chem. Phys.* **1999**, *110*, 10452–10467.
(10) Laio, A.; VandeVondele, J.; Rothlisberger, U. *J. Chem. Phys.* **2002**, *116*, 6941–6947.
(11) Hohenberg, P.; Kohn, W. *Phys. Rev. B* **1964**, *136*, 864–871.
(12) Kohn, W.; Sham, L. J. *Phys. Rev.* **1965**, *140*, 1133–1138.
(13) Nonella, M.; Mathias, G.; Eichinger, M.; Tavan, P. *J. Phys. Chem. B* **2003**, *107*, 316–322.
(14) Schmitz, M.; Tavan, P. In *Modern methods for theoretical physical chemistry of biopolymers*; Tanaka, S., Lewis, J., Eds.; Elsevier: Amsterdam, 2006; Chapter 8, pp 157−177.
(15) MacKerell, A. D.; et al. *J. Phys. Chem. B* **1998**, *102*, 3586–3616.
(16) Pearlman, D.; Case, D.; Caldwell, J.; Ross, W.; Cheatham, T., III; DeBolt, S.; Ferguson, D.; Seibel, G.; Kollman, P. *Comput. Phys. Commun.* **1995**, *91*, 1–41.
(17) van Gunsteren, W.; Daura, X.; Mark, A. *Encycl. Comput. Chem.* **1998**, *2*, 1211–1216.
(18) Babitzki, G.; Denschlag, R.; Tavan, P. *J. Chem. Phys. B* **2009**, *113*, 10496–10508.
(19) Babitzki, G.; Mathias, G.; Tavan, P. *J. Chem. Phys. B* **2009**, *113*, 10483–10495.
(20) Gascon, J. A.; Leung, S. S. F.; Batista, E. R.; Batista, V. S. *J. Chem. Theory Comput.* **2006**, *2*, 175–186.
(21) Anderson, S.; Dragnea, V.; Masuda, S.; Ybe, J.; Moffat, K.; Bauer, C. *Biochemistry* **2005**, *44*, 7998–8005.
(22) Gauden, M.; van Stokkum, I. H. M.; Key, J. M.; Lührs, D. C.; van Grondelle, R.; Hegemann, P.; Kennis, J. T. M. *Proc. Natl. Acad. Sci. U.S.A.* **2006**, *103*, 10895–10900.
(23) Unno, M.; Masuda, S.; Ono, T. A.; Yamauchi, S. *J. Am. Chem. Soc.* **2006**, *128*, 5638–5639.
(24) Yuan, H.; Anderson, S.; Masuda, S.; Dragnea, V.; Moffat, K.; Bauer, C. *Biochemistry* **2006**, *45*, 12687–12694.
(25) Grinstead, J.; Hsu, S.-T.; Laan, W.; Bonvin, A.; Hellingwerf, K.; Boelens, R.; Kaptein, R. *ChemBioChem* **2006**, *7*, 187–193.
(26) Masuda, S.; Tomida, Y.; Ohta, H.; Takamiya, K. *J. Mol. Biol.* **2007**, *368*, 1223–1230.
(27) Stelling, A.; Ronayne, K.; Nappa, J.; Tonge, P.; Meech, S. *J. Am. Chem. Soc.* **2007**, *129*, 15556–15564.
(28) Takahashi, R.; Okajima, K.; Suzuki, H.; Nakamura, H.; Ikeuchi, M.; Noguchi, T. *Biochemistry* **2007**, *46*, 6459–6467.
(29) Obanayama, K.; Kobayashi, H.; Fukushima, K.; Sakurai, M. *Photochem. Photobiol.* **2008**, *84*, 1003–1010.
(30) Bonetti, C.; Mathes, T.; van Stokkum, I. H. M.; Mullen, K. M.; Groot, M.-L.; van Grondelle, R.; Hegemann, P.; Kennis, J. T. M. *Biochem. J.* **2008**, *95*, 4790–4802.
(31) Domratcheva, T.; Grigorenko, B. L.; Schlichting, I.; Nemukhin, A. V. *Biophys. J.* **2008**, *94*, 3872–3879.
(32) Sadeghian, K.; Bocola, M.; Schütz, M. *J. Am. Chem. Soc.* **2008**, *130*, 12501–12513.
(33) Sadeghian, K.; Bocola, M.; Schütz, M. *Phys. Chem. Chem. Phys.* **2010**, *12*, 8840–8846.
(34) Masuda, S.; Hasegawa, K.; Ishii, A.; Ono, T. A. *Biochemistry* **2004**, *43*, 5304–5313.
(35) Masuda, S.; Hasegawa, K.; Ono, T. A. *Plant Cell Physiol.* **2005**, *46*, 1894–1901.
(36) Unno, M.; Sano, R.; Masuda, S.; Ono, T. A. *J. Phys. Chem. B* **2005**, *109*, 12620–12626.
(37) Hasegawa, K.; Masuda, S.; Ono, T. *Plant Cell Physiol.* **2005**, *46*, 136–146.
(38) Person, B. Resonanz-Raman-Spektroskopie zur Untersuchung der Photoreaktionen biologischer Blaulichtrezeptoren. Ph.D. thesis; Universität Bielefeld, Germany, 2007.
(39) Jung, A.; Reinstein, J.; Domratcheva, T.; Shoeman, R.-L.; Schlichting, I. *J. Mol. Biol.* **2006**, *362*, 717–732.
(40) Humphrey, W.; Dalke, A.; Schulten, K. *J. Mol. Graphics* **1996**, *14*, 33–38.
(41) Rieff, B.; Mathias, G.; Bauer, S.; Tavan, P. *Photochem. Photobiol.* **2010**, *87*, 511–523.
(42) Abe, M.; Kyogoku, Y.; Kitagawa, T.; Kawano, K.; Ohishi, N.; Takai-Suzuki, A.; Yagi, K. *Spectrochim. Acta A* **1986**, *42*, 1059–1068.
(43) Birss, V. I.; Hinman, A. S.; McGarvey, C. E.; Segal, J. *Electrochim. Acta* **1994**, *39*, 2449–2454.
(44) Kondo, M.; Neppa, J.; Ronayne, K. L.; Stelling, A. L.; Tonge, P. J.; Meech, S. R. *J. Phys. Chem. B* **2006**, *110*, 20107–20110.
(45) Hazekawa, I.; Nishina, Y.; Sato, K.; Shichiri, M.; Miura, R.; Shiga, K. *J. Biochem.* **1997**, *121*, 1147–1154.
(46) Nishina, Y.; Sato, K.; Miura, R.; Matsui, K.; Shiga, K. *J. Biochem.* **1998**, *124*, 200–208.
(47) Copeland, R.; Spiro, T. *J. Phys. Chem.* **1986**, *90*, 6654–6657.
(48) Hellwig, P.; Scheide, D.; Bungert, S.; Mäntele, W.; Friedrich, T. *Biochemistry* **2000**, *39*, 10884–10891.
(49) Wille, G.; Ritter, M.; Friedemann, R.; Mäntele, W.; Hübner, G. *Biochemistry* **2003**, *42*, 14814–14821.
(50) Nishina, Y.; Sato, K.; Setoyama, C.; Tamaoki, H.; Miura, R.; Shiga, K. *J. Biochem.* **2007**, *142*, 265–272.
(51) Wolf, M. M. N.; Schumann, C.; Gross, R.; Domratcheva, T.; Diller, R. *J. Phys. Chem. B* **2008**, *112*, 13424–13432.
(52) Jung, A.; Domratcheva, T.; Tarutina, M.; Wu, Q.; Ko, W.; Shoeman, R.; Gomelsky, M.; Gardner, K.; Schlichting, I. *Proc. Natl. Acad. Sci. U.S.A.* **2005**, *102*, 12350–12355.
(53) Mathias, G.; Egwolf, B.; Nonella, M.; Tavan, P. *J. Chem. Phys.* **2003**, *118*, 10847–10860.
(54) Niedermeier, C.; Tavan, P. *J. Chem. Phys.* **1994**, *101*, 734–748.
(55) Niedermeier, C.; Tavan, P. *Mol. Simul.* **1996**, *17*, 57–66.
(56) Allen, M. P.; Tildesley, D. *Computer Simulations of Liquids*; Clarendon: Oxford, 1987.
(57) Eichinger, M.; Grubmüller, H.; Heller, H.; Tavan, P. *J. Comput. Chem.* **1997**, *18*, 1729–1749.
(58) Grubmüller, H.; Tavan, P. *J. Comput. Chem.* **1998**, *19*, 1534–1552.
(59) Berendsen, H. J. C.; Postma, J. P. M.; van Gunsteren, W. F.; DiNola, A.; Haak, J. R. *J. Chem. Phys.* **1984**, *81*, 3684–3690.

(60) CPMD V3.9, Copyright IBM Corp 1990−2008, Copyright MPI für Festkörperforschung Stuttgart 1997−2001, see also www.cpmd.org.
(61) Troullier, N.; Martins, J. L. *Phys. Rev. B* **1991**, *43*, 1993–2005.
(62) Becke, A. D. *Phys. Rev. A* **1988**, *38*, 3098–3100.
(63) Perdew, J. P.; Yue, W. *Phys. Rev. B* **1986**, *33*, 8800–8802.
(64) Nonella, M.; Mathias, G.; Tavan, P. *J. Phys. Chem. A* **2003**, *107*, 8638–8647.
(65) Schmitz, M.; Tavan, P. *J. Chem. Phys.* **2004**, *121*, 12233–12246.
(66) Schmitz, M.; Tavan, P. *J. Chem. Phys.* **2004**, *121*, 12247–12258.
(67) Rauhut, G.; Pulay, P. *J. Phys. Chem.* **1995**, *99*, 3093–3100.
(68) Nonella, M.; Tavan, P. *Chem. Phys.* **1995**, *199*, 19–32.
(69) Neugebauer, J.; Hess, B. A. *J. Chem. Phys.* **2003**, *118*, 7215–7225.
(70) Jorgensen, W. L.; Chandrasekhar, J.; Madura, J. D.; Impey, R. W.; Klein, M. L. *J. Chem. Phys.* **1983**, *79*, 926–935.
(71) Brünger, A. X-PLOR Manual. The Howard Hughes Medical Institute and Department of Molecular Biophysics and Biochemistry, Yale University: New Haven, 1992.
(72) Kräutler, V.; van Gunsteren, W. F.; Hünenberger, P. *J. Comput. Chem.* **2001**, *22*, 501–508.
(73) Lingenheil, M.; Denschlag, R.; Reichold, R.; Tavan, P. *J. Chem. Theory Comput.* **2008**, *4*, 1293–1306.
(74) Liu, P.; Kim, B.; Friesner, R. A.; Berne, B. J. *Proc. Natl. Acad. Sci. U.S.A.* **2005**, *102*, 13749.
(75) Denschlag, R.; Lingenheil, M.; Tavan, P.; Mathias, G. *J. Chem. Theory Comput.* **2009**, *5*, 2847–2857.
(76) Singh, U. C.; Kollman, P. A. *J. Comput. Chem.* **1984**, *5*, 129–145.
(77) Höchtl, P.; Boresch, S.; Bitomsky, W.; Steinhauser, O. *J. Chem. Phys.* **1998**, *109*, 4927–4937.
(78) Richardi, J.; Fries, P.; Millot, C. *J. Mol. Liq.* **2005**, *117*, 3–16.
(79) Guillot, B. *J. Mol. Liq.* **2002**, *101*, 219–260.
(80) Grinstead, J.; Avila-Perez, M; Hellingwerf, K.; Boelens, R.; Kaptein, R. *J. Am. Chem. Soc.* **2006**, *128*, 15066–15067.
(81) Unno, M.; Kikuchi, S.; Masuda, S. *Biophys. J.* **2010**, *98*, 1949–1956.
(82) VandeVondele, J.; Krack, M.; Mohamed, F.; Parrinello, M.; Chassaing, T.; Hutter, J. *Comput. Phys. Commun.* **2005**, *167*, 103–128.